Thermal Dehydration of Hydrated Salts During Fire Exposure and Its Role in Predicting the Performance of Gypsum Based Systems

Maximilian Pache *, Michaela D. Detsi, Ioannis D. Mandilaras, Dimos A. Kontogeorgos, Maria A. Founti

Posted Date: 9 March 2026

doi: 10.20944/preprints202603.0582.v1

Keywords: gypsum-based materials; flame-retardant additives; dehydration kinetics; Avrami–Erofeev model; solid-state reactions; isoconversional analysis; multi-step reaction modeling

 doi:10.20944/preprints202603.0582.v1

Article

Thermal Dehydration of Hydrated Salts During Fire Exposure and Its Role in Predicting the Performance of Gypsum Based Systems

Maximilian Pache *, Michaela D. Detsi, Ioannis D. Mandilaras, Dimos A. Kontogeorgos and Maria A. Founti

Laboratory of Heterogeneous Mixtures and Combustion Systems, School of Mechanical Engineering, National Technical University of Athens, Heroon Polytechniou 9, Zografou Campus, Athens 15780, Greece

* Correspondence: maximiliankuhn@mail.ntua.gr

Abstract

Gypsum based fire protection relies on thermally activated dehydration, where chemically bound water is released and evaporated, producing an endothermic heat sink and delaying heat penetration through assemblies. In parallel, non-organic hydrated salts are increasingly used as flame retardant additives in gypsum-based systems to enhance heat absorption over targeted temperature ranges. Fire simulation tools and performance-based fire engineering methods require dehydration kinetics and reaction enthalpies that can be implemented as coupled thermal chemical source terms. However, additive specific kinetic datasets suitable for such implementation remain limited, especially under restricted vapor exchange conditions representative of porous construction materials. The present study investigates the thermal decomposition behavior and dehydration kinetics of selected non-organic hydrated salts—aluminium trihydrate (ATH), magnesium hydroxide (MDH), calcium aluminate sulphate (CAS), and magnesium sulphate heptahydrate (ESM)—commonly used as flame-retardant additives in gypsum-based construction materials. Differential scanning calorimetry (DSC) experiments were conducted at three heating rates (10, 20, and 30 K/min for MDH, CAS and ESM and 20, 40 and 60 K/min for GB-ATH) up to 600 °C using pinhole crucibles to simulate autogenous vapor pressure. Thermal analysis revealed that ATH, MDH, and CAS undergo single-step dehydration, while ESM exhibits a complex multi-step mechanism involving the formation of intermediate meta-stable hydrates. Kinetic parameters were determined using both model-free (Starink) and model-fitting approaches. The derived activation energy profiles confirmed the single-step nature of ATH and MDH and identified CAS and ESM as multi-stage systems. All reactions were well described using the Avrami–Erofeev model, indicating nucleation-and-growth mechanisms. The extracted kinetic triplets were validated through numerical simulation, showing close agreement with experimental α(t) and dα/dt(T) data. The resulting kinetic triplets and dehydration enthalpies form a directly usable dataset for coupled heat transfer and dehydration models of gypsum-based assemblies, enabling improved parameterization of endothermic heat sinks and bound water release in fire safety engineering simulations.

Keywords: gypsum-based materials; flame-retardant additives; dehydration kinetics; Avrami–Erofeev model; solid-state reactions; isoconversional analysis; multi-step reaction modeling

1. Introduction

Gypsum boards are widely recognized for their ability to withstand high temperatures, primarily due to a thermally activated dehydration mechanism. When heated, chemically bound water is released from their crystal structure and evaporates, absorbing substantial amounts of heat and delaying the progression of fire through building components . The role of dehydration and coupled moisture transport in gypsum board thermal behavior has been demonstrated in

 doi:10.20944/preprints202603.0582.v1

experimental and modelling studies, including effects on effective heat capacity and thermal response under fire exposure conditions [1–11].

In recent years, non-organic hydrated salts have gained attention as complementary flame-retardant additives in gypsum-based systems. Compounds such as Aluminium Trihydrate (ATH), Magnesium Hydroxide (MDH), Calcium Aluminate Sulphate (CAS), and Magnesium Sulphate Heptahydrate (ESM) exhibit similar endothermic dehydration behavior, contributing significantly to thermal inertia during fire exposure [12–21].

While the thermal performance of gypsum has been extensively investigated, the dehydration kinetics and thermochemical behavior of these salt additives remain less well characterized, especially when they are incorporated inside gypsum boards. Understanding their behavior is essential for accurate modeling in fire safety simulations, particularly as direct experimental data at elevated temperatures are often difficult and expensive to obtain [5,11,22–26].

The objective of the work is to quantify dehydration enthalpies and to derive kinetic triplets for ATH, MDH, CAS, and ESM under controlled DSC conditions with restricted vapor exchange, intended to approximate the confined vapor environment relevant to porous gypsum systems. The study provides a dataset of additive specific dehydration kinetics derived using both iso-conversional analysis and model fitting in accordance with guidance issued by the Kinetics Committee of the International Confederation for Thermal Analysis and Calorimetry (ICTAC) [39–42]. The resulting parameters are positioned as effective modelling inputs for coupled thermal chemical fire models of gypsum-based assemblies, supporting the implementation steps and sensitivity analyses needed in engineering practice

The work contributes to the science and technology of fires by linking fundamental thermal decomposition kinetics with the predictive assessment of fire performance in gypsum-based construction systems. By quantifying dehydration mechanisms under fire-relevant heating conditions, the paper provides material-level parameters that can be integrated into fire modelling frameworks. The generated kinetic datasets provide physically grounded inputs for performance based fire modelling, enabling improved prediction of heat transfer, structural protection, and fire spread in building assemblies [27]. By translating laboratory scale thermal analysis into parameters relevant for fire safety engineering, the work contributes to bridging material science with applied fire technology and supports the development of resilient construction strategies that mitigate fire impacts on communities and the built environment.

2. Thermochemistry of the Investigated Hydrated Salts

2.1. Aluminum Trihydrate (ATH)

Aluminium Trihydrate (ATH) is a crystalline form of aluminium hydroxide that begins to decompose thermally above 200 °C, releasing water and yielding aluminium oxide (Al_2O_3) as the solid residue [23,24,26]. Depending on specific conditions, this dehydration process is described in the literature either as a single-step [23,24,26,28] or multi-step reaction [29–31], typically occurring within the temperature range of 200 °C to 350 °C (see eq. (1)), where $\Delta H_{dh\text{-}ATH}$ is the energy absorbed the reaction.

$$Al(OH)_3(s)+\Delta H_{dh\text{-}ATH} \rightarrow 1/2\, Al_2O_3(s)+3/2\, H_2O(g), \quad (1)$$

2.2. Magnesium Hydroxide (MDH)

In contrast, Magnesium Hydroxide (MDH) undergoes thermal decomposition at higher temperatures—between 350 °C and 550 °C—producing magnesium oxide (MgO) and water vapor. The transformation is generally regarded as a single-step reaction [12,14,15,30,32], characterized by a distinct endothermic peak and a well-defined enthalpy change, denoted $\Delta H_{dh\text{-}MDH}$ (see eq. (2)).

$$Mg(OH)_2(s)+\Delta H_{dh\text{-}MDH} \leftrightarrow MgO(s)+H_2O(g), \quad (2)$$

 doi:10.20944/preprints202603.0582.v1

2.3. Calcium Aluminate Sulphate (CAS, Ettringite Related)

Calcium Aluminate Sulphate (CAS), a compound structurally related to ettringite, has been studied extensively in the context of cement hydration, where it is known for its delayed expansion phenomena. However, its thermal behavior under fire conditions remains less well documented [13,16]. CAS dehydrates over a broad temperature range, roughly 30 °C to 300 °C [33], releasing water vapor and leaving behind calcium sulfoaluminate ($CaOxAl_2O_3x3CaSO_4$) as the primary residue (see eq. (3)), where $\Delta H_{dh\text{-}CAS}$ is the energy absorbed during the reaction.

$$3CaO*Al_2O_3*3CaSO_4*32H_2O+\Delta H_{dh\text{-}CAS}\rightarrow 3CaO*Al_2O_3*3CaSO_4(s)+32H_2O(g), \quad (3)$$

Research has shown that the dehydration of ettringite and related phases—sometimes collectively termed "meta-ettringite"—proceeds through multiple intermediates. For example, Rubinaite et al. observed that calcium monosulfoaluminate can rehydrate into ettringite at water vapor pressures exceeding 0.753 p/p_0, emphasizing the role of ambient humidity on phase stability and transformation kinetics [20]. Here, p/p_0 denotes the ratio between the actual water vapour pressure and the saturation vapour pressure at the same temperature, corresponding to the relative humidity. Based on the earlier work of Šatava and Vepřek [19], Chen [13] summarizes a three-stage dehydration pathway for these systems, extending up to ~232 °C (eq. 4). [20]. Based on the earlier work of Šatava and Vepřek [19], Chen [13] summarizes a three-stage dehydration pathway for these systems, extending up to ~232 °C (eq. (4)).

$$C_6A\bar{S}H_{32}(s)\rightarrow C_4A\bar{S}H_{32}(s)(\text{monosulfate})+2C\bar{S}H_{0.5}+19H\ (1),\ 111<T<190\ °C$$

$$C_4A\bar{S}H_{12}(s)\rightarrow C_3A\bar{S}H_6(s)+C\bar{S}(s)+6H\ (1),\ 190<T<280\ °C \quad (4)$$

$$3C_3A\bar{S}H_6(s)\rightarrow C_4A_3H_3(s)+5CH(s)+10H\ (1),\ T>280\ °C$$

Magnesium Sulfate Heptahydrate (ESM) displays a particularly complex thermal decomposition pathway. Dehydration occurs between 50 °C and 300 °C and proceeds through several intermediate hydrates before forming anhydrous magnesium sulfate ($MgSO_4$) [34–38]. The individual dehydration steps involve the sequential loss of water molecules, and the reaction behavior is strongly influenced by the internal water vapor pressure developed within and around the sample [12,38]. The associated enthalpy change/energy absorption for the global process is represented as $\Delta H_{dh\text{-}ESM}$ is (eq.5).

$$MgSO_4\,7H_2O(s)+\Delta H_{dh\text{-}ESM}\rightarrow MgSO_4(s)+7H_2O(g), \quad (5)$$

3. Solid State Kinetics

Solid-state chemical kinetics examines how various factors influence the rate at which reactions proceed, offering key insights into underlying mechanisms and transition states [39]. For reversible reactions involving a solid reactant and a gaseous product—typically represented as ($A_{solid} \Leftrightarrow B_{solid} + C_{gas}$) —the transformation rate is commonly governed by three core variables: the temperature-dependent rate constant $k(T)$, the conversion-dependent reaction model $f(\alpha)$, and the pressure function $h(P)$, which accounts for the influence of gas-phase species on the reaction environment (see eq. 6) [40].

$$\frac{d\alpha}{dt}=k(T)f(\alpha)h(P), \quad (6)$$

In solid-state reactions that produce gaseous products, the influence of gas-phase pressure on reaction kinetics becomes particularly relevant. The ICTAC Kinetics Committee has provided guidance on this matter, noting that under typical experimental conditions—such as those in DSC or TGA crucibles—direct measurement of partial pressures is often impractical or impossible [40]. As a result, the pressure-dependent term $h(P)$ from the general rate expression (eq. 6) is frequently

 doi:10.20944/preprints202603.0582.v1

omitted, and its effect is instead implicitly absorbed into the temperature-dependent rate constant *k(T)*.

Under such assumptions, the reaction rate can be described by a modified Arrhenius-type equation (eq. 7), where *A* denotes the pre-exponential factor, E_a the activation energy, R_g the universal gas constant, *f(α)* the kinetic model, and *α* the conversion fraction, which progresses from 0 (unreacted) to 1 (fully reacted). When pressure effects are significant but unmeasured, the extracted kinetic parameters A and E_a should be interpreted as effective values that inherently reflect the closed or semi-closed nature of the experimental system.

$$\frac{d\alpha}{dt} = k(T)f(\alpha) = Ae^{-\left(E_a/R_gT\right)}f(\alpha), \quad (7)$$

The functional form of the reaction model f(*α*)—which governs how the reaction rate evolves with conversion—can generally be grouped into three kinetic profiles [40]:

- Accelerating models, in which the reaction rate increases steadily and peaks toward the end of the transformation;
- Decelerating models, where the rate is initially high and gradually declines;
- Sigmoidal (autocatalytic) models, which exhibit an S-shaped rate curve, characterized by an initial acceleration followed by deceleration.

These classifications, especially relevant under isothermal conditions, are derived from the shapes of the *α*(t) curves (with t denoting time) or, in non-isothermal experiments, from the corresponding *α*(T) or d*α*/dT profiles, where temperature replaces time via the heating rate. They correspond to various mechanistic interpretations, often implemented through kinetic models such as the power-law, nth-order, diffusion-controlled, or nucleation-and-growth frameworks—including the Avrami–Erofeev model [40–42]. Specifically:

- Nucleation models assume the reaction initiates at discrete sites and propagates via growth of product phases;
- Geometrical contraction models describe transformations where the reaction front moves inward from the particle surface;
- Diffusion models reflect rate control by mass transport of species;
- and reaction-order models apply the classical kinetics of homogeneous systems to solid-state processes.

According to the framework established by the ICTAC Kinetics Committee [40,43], the overall rate of a multi-step solid-state reaction can be described as a weighted sum of individual reactions, as expressed in equation (8). Here, NR denotes the total number of reaction steps, while w_r and α_r represent the normalized weight fraction ($\sum w_r = 1$) and the conversion degree of each individual process, respectively [11].

$$\frac{d\alpha}{dt} = \sum_{r=1}^{N_R} w_r \frac{d\alpha_r}{dt}, \quad (8)$$

To capture the underlying reaction dynamics, each step can be characterized by its own kinetic triplet: the activation energy (E_a), the pre-exponential factor (A), and the reaction model f(*α*) [40,43–45]. While idealized systems may follow a single kinetic pathway, most real-world solid-state reactions—especially those involving hydrated salts or composite materials—require multiple kinetic triplets to adequately reflect overlapping or sequential thermal events [40,44].

Experimental determination of these kinetic parameters relies on thermal analysis techniques such as DSC, TGA, or DTA, which generate both integral and differential signal data [40,44]. The fidelity of the derived kinetic values is closely tied to data quality and noise levels, though numerical methods allow transformation between data formats to suit either integral or differential evaluation strategies [40].

 doi:10.20944/preprints202603.0582.v1

Approaches to kinetic analysis fall broadly into two categories: model-free (isoconversional) and model-fitting. Model-free methods, such as the Starink approach, estimate activation energy directly as a function of the conversion degree, without presuming a specific reaction mechanism. This makes them particularly suited for complex systems with multiple, overlapping transformations—such as those observed in coal pyrolysis or salt hydrates [46,47].

In contrast, model-fitting techniques compare experimental data to predefined kinetic models, yielding all three elements of the kinetic triplet. While this method can produce excellent agreement with data, it may lead to ambiguous or model-dependent parameter estimates, especially when only single heating rate experiments are available. As highlighted by Kontogeorgos [44], different models may fit the same dataset equally well, leading to potential misinterpretations of underlying reaction mechanisms.

In the present study, both model-free and model-fitting methods are employed to determine the kinetic triplets for the investigated salts, following the methodological standards and best practices outlined by the ICTAC Committee [40].

4. Materials and Methods

4.1. DSC Experiments and Baseline Processing; Specimens, Heating Rates, and Replication

To investigate the dehydration kinetics of the selected non-organic salts, Differential Scanning Calorimetry (DSC) was employed under controlled laboratory conditions.

All measurements followed the experimental protocol described by Kontogeorgos [44] using a Star^{e} SW 8.10 Mettler Toledo DSC system with a temperature accuracy of ±2%. Samples were heated in an inert nitrogen atmosphere with a flow rate of 100 ml/min, using sealed 40 µl aluminum crucibles. The temperature range extended up to 600 °C, and the instrument was calibrated at two reference points—156.6 °C (indium) and 419.6 °C (zinc)—to determine sensitivity and ensure consistent baseline stability [44].

Prior to each experiment, a baseline measurement was recorded using an empty crucible under identical conditions. This baseline was subtracted from the sample data to eliminate instrumental artifacts. Tangential integration baselines were applied to define the thermal event intervals relevant to each reaction.

To simulate autogenous vapor pressure conditions during dehydration, all samples were measured in pinhole-lid crucibles (1 mm diameter), thereby restricting vapor exchange with the surroundings. This configuration allows the buildup of internally generated water vapor, which is known to influence the dehydration pathway and reaction kinetics of calcium sulfate dihydrate, including the occurrence of one- or two-step mechanisms depending on the prevailing vapor partial pressure [22,44]. Although water vapor pressure was not directly monitored, its influence is implicitly reflected in the calculated kinetic parameters (A and E_a), in accordance with ICTAC recommendations for closed-system approximations [40,48].

Each salt was analyzed at three different linear heating rates, in line with ICTAC guidelines for kinetic evaluation [40]. The temperature program ranged from 25 °C to 600 °C. For ATH, due to handling limitations of the pure material, a gypsum board containing 5 wt.% ATH was used. A 10 cm × 10 cm section of the board was sampled, crushed, and ground into powder. The other salts (MDH, CAS, ESM) were analyzed in their as-received powdered form.

Sample masses and heating rates for each run are listed in Table 1. Mass variations across runs remained within ±5%, which is acceptable for kinetic computations under ICTAC methodology [36].

Table 1. This is a table. Tables should be placed in the main text near to the first time they are cited.

Sample	ß (K min^{-1})	m (mg)
	20	13.89

 doi:10.20944/preprints202603.0582.v1

GB-ATH[1]	40	13.59
	60	13.62
MDH	2	14.87
	10	14.69
	20	14.19
CAS	2	10.52
	10	10.22
	20	10.24
ESM	2	14.37
	10	12.51
	20	14.20

[1] GB-ATH stands for the gypsum board sample containing 5% of ATH.

Each DSC condition was repeated three times. The observed reproducibility error was within acceptable instrument limits and did not exceed 7.2%.

4.2. Kinetic Analysis Tools and Procedures

To determine the chemical kinetics of the investigated solid-state dehydration reactions (Equations 1–5), the in-house developed ChemKin Toolbox was employed, following the kinetic analysis framework previously established for gypsum dehydration reactions, including model-free and model-fitting approaches for the determination of the kinetic triplet [6,10]. This software suite, created at the Laboratory of Heterogeneous Mixtures & Combustion Systems at the National Technical University of Athens, enables extraction of kinetic parameters from DSC and TGA data in accordance with the recommendations of the ICTAC Kinetics Committee [39]. The toolbox supports the resolution of up to eight consecutive or overlapping reaction steps per material.

5. Results

5.1. Thermal Dehydration Behavior

Figure 1 presents the DSC results obtained for four test materials: a gypsum board containing 5 wt.% ATH (Figure 1a), and the pure compounds MDH (Figure 1b), CAS (Figure 1c), and ESM (Figure 1d). Across all specimens, the DSC curves exhibit comparable shapes at different heating rates, with the expected shift of peak temperatures toward higher values as the heating rate increases.

To ensure the reliability of the measurements, each experiment was performed three times, and the reported results represent the average of the three runs. Minor variations between replicates—primarily due to slight differences in sample mass (see Table 1) or in the selection of the integration range for thermal events—were observed but remained within acceptable limits. These deviations had no discernible impact on the subsequent kinetic evaluation.

In the DSC profile of the gypsum board containing 5 wt.% ATH (Figure 1a), the characteristic two-step dehydration of calcium sulphate dihydrate is evident below 250 °C. In this sequence, the material initially loses approximately 75% of its hydration water, forming calcium sulphate hemihydrate (bassanite), followed by further dehydration to the soluble anhydrite III phase. This two-stage process has been well documented and was confirmed here through peak deconvolution, which enabled the resolution of overlapping thermal events. The first transition follows a two-dimensional nucleation and growth mechanism, while the second is governed by a three-dimensional pathway, consistent with previous kinetic analyses [47].

 doi:10.20944/preprints202603.0582.v1

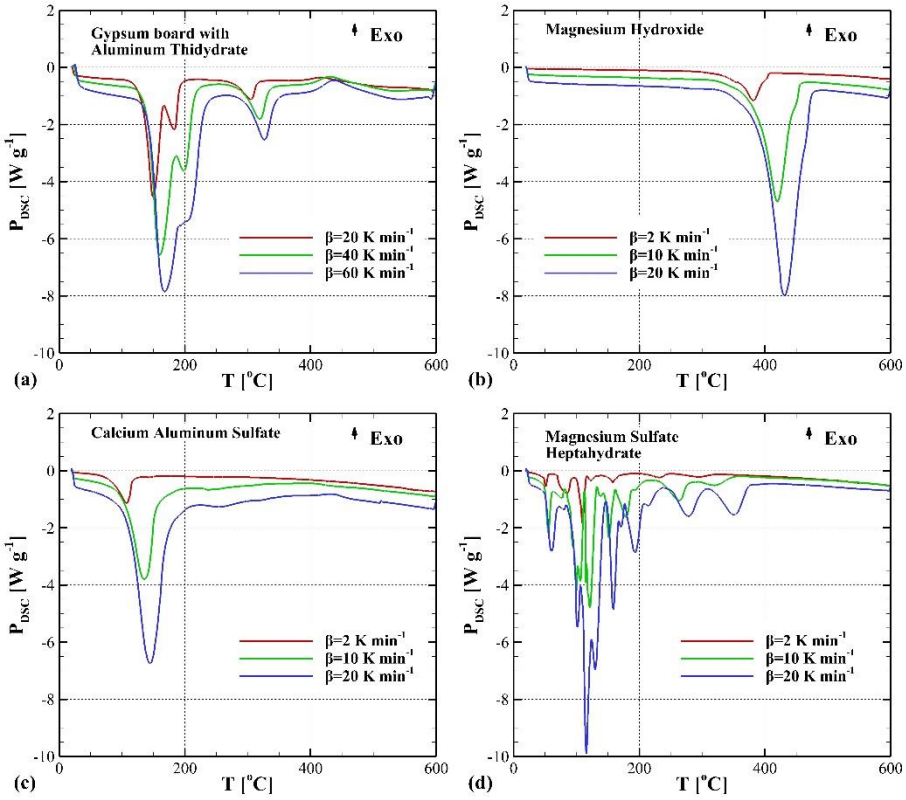

Figure 1. DSC curves as a function of sample temperature for a) GB-ATH, b) MDH, c) CAS, and d) ESM at different heating rates.

Additionally, a minor exothermic signal near 420 °C was observed, corresponding to the irreversible transformation of anhydrite III into the more stable anhydrite II phase via structural reorganization (hexagonal to orthorhombic).

Notably, the present measurements revealed a previously unreported high-temperature endothermic peak between 300 °C and 350 °C. This distinct signal is attributed to the dehydration of aluminium trihydrate and represents a new observation within gypsum board systems. Based on its thermal profile and sharpness, this process is likely governed by a single-step mechanism, as described in equation (1).

The DSC curve of pure magnesium hydroxide (MDH), shown in Figure 1b, exhibits a single pronounced endothermic peak in the range of 380 °C to 420 °C, with the exact position depending on the applied heating rate. This thermal event corresponds to the dehydration of MDH and is characteristic of a single-step reaction mechanism, as defined in equation (2).

A comparable thermal signature is observed in the case of calcium aluminate sulphate (CAS) (Figure 1c). The DSC curve reveals a single endothermic peak between 100 °C and 150 °C, again shifting with the heating rate. This behavior suggests that CAS, like MDH and ATH, undergoes a one-step dehydration reaction, as outlined in equation (3).

These results confirm that all three materials—MDH, ATH, and CAS—exhibit clearly defined, singular thermal decomposition processes under the studied conditions, supporting their classification as single-stage dehydration systems within their respective temperature domains.

The DSC results for magnesium sulphate heptahydrate (ESM), shown in Figure 1d, reveal a sequence of multiple endothermic peaks, indicating a complex multi-step dehydration mechanism. These thermal events are attributed to the stepwise release of water molecules and the formation of intermediate meta-stable hydrates during the decomposition process [30,31,33,37]. This behavior is strongly influenced by local water vapor pressure within the sample environment. Rubinaite et al. [20] demonstrated that the stability and transformation pathways of similar hydrates—such as calcium monosulfoaluminate—are highly sensitive to ambient p/p_0 conditions. Their work showed

 doi:10.20944/preprints202603.0582.v1

that varying vapor pressures can shift the dominant reaction products between gypsum, hemihydrate, and ettringite, underscoring the critical role of moisture in phase evolution.

Based on the observed DSC profiles, CAS and ESM dehydrate primarily in the low-temperature range of 100 °C to 250 °C, while ATH and MDH exhibit thermal activity at elevated temperatures between 250 °C and 450 °C. Accordingly, CAS and ESM can be categorized as low-temperature dehydrating salts, whereas ATH and MDH fall into the high-temperature class.

Table 2 summarizes the measured mass loss (Δ_m) and the corresponding thermal effects recorded during the DSC experiments. The reported Δ_m values reflect the total weight reduction of each sample between ambient temperature and 600 °C. The table also lists the energy quantities associated with three distinct processes:

- ΔH_{GB}: heat absorbed during the two-step dehydration of gypsum boards,
- ΔH_R: exothermic reorganization from anhydrite III to anhydrite II,
- ΔH_{add}: heat absorbed due to the dehydration of the added salts ATH, MDH, CAS, and ESM.

Table 2. Mass loss and energy absorbed/produced for each DSC measurement and specimen.

Sample	β (K min^{-1})	Δm[(2)] (mg)	Δm[(2)] (%)	ΔH[(3)] (kJ kg^{-1})	ΔH[(4)] (kJ kg^{-1})	ΔH[(5)] (kJ kg^{-1})
GB-ATH[(1)]	20	2.54	18.29	-377.56	-48.45	9.15
	40	2.58	18.98	-386.00	-50.55	13.92
	60	2.55	18.72	-381.05	-48.40	14.10
MDH	2	4.13	27.77		-1077.38	
	10	3.98	27.09		-1100.32	
	20	3.77	26.57		-1092.89	
CAS	2	4.23	40.21		-729.52	
	10	4.13	40.41		-713.28	
	20	4.12	40.23		-712.06	
ESM	2	7.34	51.08		-1120.84	
	10	6.34	50.68		-1103.95	
	20	7.22	50.85		-1106.10	

[1]GB-ATH stands for the gypsum board sample containing 5% of ATH. [2] Δm stands for the total mass loss of the examined samples (mass sample at 600 oC). [3]ΔH stands for the energy absorbed due to the two-step dehydration process of gypsum boards. [4]ΔH stands for the energy absorbed due to the dehydration of the examined additives, i.e. ATH, MDH, CAS and ESM. [5]ΔH stands for the energy produced due to the crystal reorganization reaction of gypsum boards.

The average energy values for the additives are as follows:

- $\Delta H_{ATH} = 982.67 \pm 73.63$ kJ/kg,
- $\Delta H_{MDH} = 1090.20 \pm 35.11$ kJ/kg,
- $\Delta H_{CAS} = 718.29 \pm 29.24$ kJ/kg,
- $\Delta H_{ESM} = 1110.30 \pm 27.58$ kJ/kg.

These values are in excellent agreement with literature data for the respective materials [12–15,22,23,25,27–32,34,48–52], confirming the accuracy of the present measurements. Notably, ATH, MDH, and ESM exhibit significantly higher enthalpies of dehydration compared to CAS. This suggests that these three salts are thermally more efficient in terms of heat absorption and are therefore better suited as flame-retardant additives in gypsum-based systems.

 doi:10.20944/preprints202603.0582.v1

5.2. Kinetic Parameters

5.2.1. Conversion Curves and Model Selection

Figure 2 shows the α-curves for ATH (Figure 2a), MDH (Figure 2b), CAS (Figure 2c), and ESM (Figure 2d). As it is shown, the dehydration reactions of ATH, MDH, and CAS exhibit sigmoidal α(T) curves, indicative of single-stage processes. In contrast, the curve for ESM displays multiple slope changes over the conversion range, suggesting the presence of several overlapping steps. This observation aligns with earlier reports on the multistep nature of ESM dehydration [37].

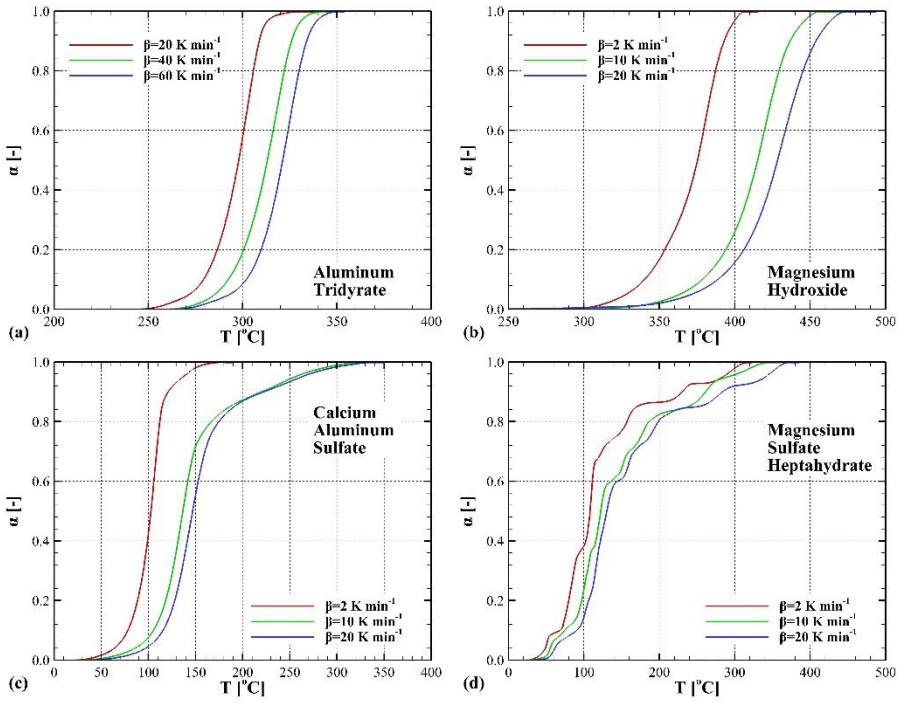

Figure 2. Conversion fraction of dehydration of a) ATH, b) MDH, c) CAS and d) ESM, at different heating rates, as a function of sample temperature.

Such complex reaction profiles benefit from kinetic deconvolution techniques, which allow for the separation of overlapping thermal events into individual steps with distinct kinetic descriptors [45]. The α(T) data served as the foundation for the kinetic parameter estimation in the subsequent modeling phase.

The choice of the Avrami–Erofeev model was guided not merely by statistical fit quality but by the sigmoidal nature of the α(T) curves observed for ATH, MDH, and CAS (see Figure 2). Such curve profiles are characteristic of nucleation-and-growth mechanisms and are well aligned with the classification schemes recommended by the ICTAC Kinetics Committee [39,46] and previously employed by Kontogeorgos [6].

To validate this mechanistic assumption, a non-linear multi-step fitting procedure was applied using the ChemKin Toolbox. The software evaluates competing kinetic models—such as Avrami–Erofeev, diffusion-controlled, and nth-order reaction schemes—and selects the most appropriate one for each reaction step. This approach allows not only for parameter estimation but also for informed model discrimination based on both physical interpretability and numerical performance.

5.2.2. Evaluation of Activation Energy

To extract the kinetic parameters of the dehydration reactions, both model-free and model-fitting approaches were applied to the experimental data presented in Figure 2. All calculations were conducted using the ChemKin Toolbox in accordance with ICTAC Kinetics Committee guidelines

 doi:10.20944/preprints202603.0582.v1

[39]. Among the model-free methods, isoconversional techniques such as those proposed by Boswell, Tang, and Starink have proven effective in handling multistep processes with overlapping reaction events [45], including complex systems like coal pyrolysis [44].

In this study, the integral isoconversional method of Starink [53] was employed to calculate the activation energy (E_a) as a function of the conversion fraction (α) over the range $0.05 \leq \alpha \leq 0.95$, using a step size of $\Delta\alpha = 0.05$. The results are summarized in Figure 3 for all four materials.

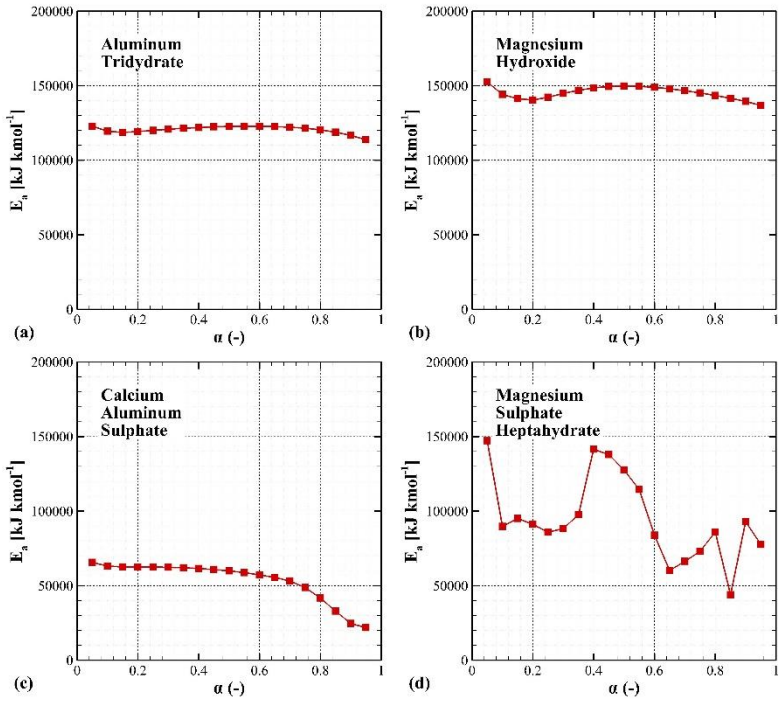

Figure 3. Activation energy of dehydration of a) ATH, b) MDH, c) CAS and d) ESM as a function of the conversion fraction.

For ATH (Figure 3a) and MDH (Figure 3b), the E_a values remain relatively stable across the full conversion range, indicating that both reactions can be considered single-step processes. This interpretation is supported by previous findings for gypsum-based systems [47] and further confirmed by the narrow spread between minimum and maximum E_a values: 7.45% for ATH and 10.80% for MDH, well within the 20–30% threshold defined for single-stage mechanisms [39].

In contrast, the dehydration of CAS and ESM shows a pronounced dependence of E_a on α (Figures 3c and 3d), with variations of 81.62% and 108.98% relative to the respective mean values. These findings provide strong evidence for a multistep mechanism in both cases.

Particularly in the case of CAS, the isoconversional analysis reveals complexities that are not apparent from the DSC curves alone. The gradual release of water and the likely formation of intermediate meta-stable hydrates—driven by changes in autogenous vapor pressure—highlight the limitations of relying solely on thermal peak analysis. These multistage characteristics are further illustrated in the mechanistic scheme of equation (9).

$$3CaO\ ^*Al_2O_3{}^*3CaSO_4{}^*32H_2O + \Delta H_{dh\text{-}CAS} \rightarrow 3CaO^*Al_2O_3{}^*3CaSO_4 x H_2O(s) + (32 - x)H_2O(g), \quad (9)$$

5.2.3. Multi-step Fitting and Model Validation

Based on the non-linear model-fitting approach [39], kinetic parameters for all five dehydration reactions (equations 1–5) were derived from the experimental DSC data. The results are summarized in Table 3. For ATH and MDH, the model-fitting analysis confirmed a single-step reaction

 doi:10.20944/preprints202603.0582.v1

mechanism, best described by the Avrami–Erofeev model. This aligns with the observed sigmoidal α(T) profiles and reflects nucleation-and-growth behavior during the conversion of aluminium trihydrate to Al_2O_3 and magnesium hydroxide to MgO, respectively.

Table 3. Kinetic parameters for the ATH, MDH, CAS and ESM dehydration reaction, obtained using the model-fitting method.

Material	Reaction ID	Weight Factor (-)	Ea (J mol-1)	A (s-1)	Reaction Model	n
ATH	I	1.000	120583.02	0.1286×10^{10}	Avrami-Erofeev	2.00
MDH	I	1.000	142500.00	0.3681×10^{9}	Avrami-Erofeev	1.35
CAS	I	0.200	35078.66	0.1660×10^{2}	Avrami-Erofeev	1.00
	II	0.100	45736.30	0.1607×10^{4}		1.25
	III	0.700	53064.64	0.4624×10^{5}		1.60
ESM	I	0.080	80000.00	0.7339×10^{11}	Avrami-Erofeev	2.50
	II	0.050	79500.00	0.1296×10^{11}		1.80
	III	0.160	91000.00	0.8074×10^{11}		2.20
	IV	0.280	98800.00	0.1765×10^{12}		2.20
	V	0.100	112000.00	0.7879×10^{12}		2.40
	VI	0.155	75000.00	0.3877×10^{7}		1.20
	VII	0.105	117000.00	0.2489×10^{10}		1.25
	VIII	0.070	108000.00	0.1862×10^{8}		1.20

In contrast, the dehydration of CAS and ESM required multi-step modeling. CAS was best represented by a three-stage mechanism, while ESM involved eight distinct reaction steps. These findings correlate with the sequential release of water and the formation of intermediate meta-stable hydrates, influenced by the build-up of water vapor pressure within the crucible during heating.

Similar behavior has been reported by Rubinaite et al. [20], who identified humidity-dependent intermediates such as hemicarbonate and calcium sulfoaluminate 14-hydrate during the carbonation of related materials. Their results underline the critical role of ambient vapor pressure in phase stability and transformation kinetics.

As noted above, all individual reaction steps identified in the multi-stage modeling of CAS and ESM were best described by the Avrami–Erofeev model, reinforcing the interpretation that nucleation and growth govern the formation of intermediate hydrate phases during dehydration.

Figure 4 presents a comparison between the predicted conversion fraction α(T) (Figures 4a–4d) and the reaction rate dα/dt(T) (Figures 4e–4h) for ATH, MDH, CAS, and ESM, using the kinetic parameters derived from the model-fitting procedure. The numerical predictions match the experimental DSC data closely across all heating rates, indicating high predictive accuracy of the extracted parameter sets.

 doi:10.20944/preprints202603.0582.v1

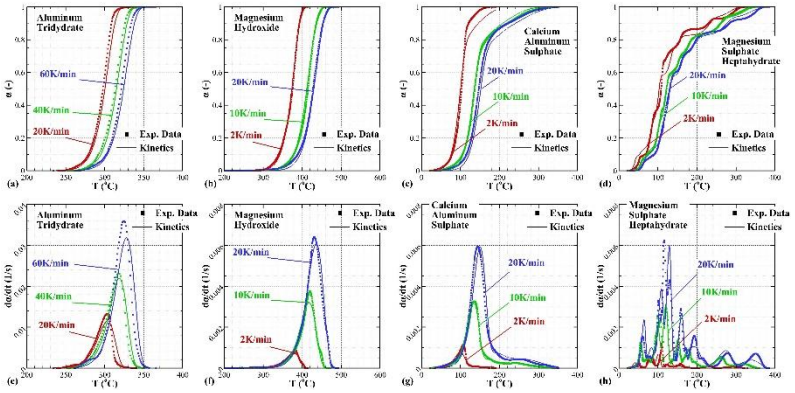

Figure 4. Comparison between the predictions (lines) and the experimental data (symbols) for different heating rates for the dehydration of ATH, MDH, CAS and ESM: up) conversion fraction and (down) reaction rate.

The best agreement is observed for ATH, MDH, and CAS, while minor deviations in the ESM results can be attributed to (a) the definition of temperature intervals for α(T) computation, (b) the choice of α-ranges assigned to specific sub-reactions during kinetic decomposition, and (c) limitations in the numerical optimization algorithm.

Overall, the consistency between simulated and measured data confirms both the reliability and physical relevance of the determined kinetic triplets. The quality of fit for both α(T) and dα/dt(T) complies with the benchmark criteria set by the ICTAC Kinetics Committee [39,46] and reflects the methodological rigor described by Kontogeorgos [6].

6. Discussion

6.1. Kinetic Implications

The thermal dehydration behaviour of hydrated salts plays a fundamental role in the fire performance of gypsum-based systems, as the release of chemically bound water governs both the endothermic heat absorption and the evolution of water vapour during fire exposure. This work investigated the kinetic characteristics of several hydrated salts using differential scanning calorimetry and model-based kinetic analysis. The results reveal clear differences in the dehydration mechanisms of the investigated materials, which have direct implications for their behaviour under elevated temperatures.

The analysed hydroxide-based systems, particularly MDH and GB-ATH, exhibited dehydration behaviour that can be approximated by a single dominant reaction step within the investigated temperature range. The relatively stable activation energy profiles obtained for these materials indicate that their dehydration is largely controlled by a single kinetic mechanism. Such behaviour is typically associated with nucleation and growth processes that can be adequately described by Avrami–Erofeev type reaction models. In contrast, the investigated sulfate-based systems, including CAS and ESM, showed clear evidence of multi-step dehydration behaviour. The variation of the apparent activation energy with increasing conversion suggests the presence of overlapping reaction processes, which may correspond to the sequential release of crystallization water or structural transformations within the solid matrix. These observations highlight the complexity of dehydration processes in multi-hydrated mineral systems and underline the limitations of simplified single-step kinetic descriptions.

The kinetic analysis further demonstrates that the assumption of a constant activation energy may not be sufficient to accurately represent the thermal decomposition of complex hydrated salts. In particular, the conversion-dependent activation energy profiles obtained for CAS and ESM indicate that the reaction pathway evolves during the dehydration process. This behaviour reflects structural rearrangements within the crystal lattice and changes in the rate-controlling mechanism as

 doi:10.20944/preprints202603.0582.v1

dehydration progresses. Consequently, kinetic models that account for variable activation energies provide a more realistic description of the dehydration process and allow a better representation of the experimental conversion curves.

6.2. Fire Engineering Interpretation of the Results

From a fire engineering perspective, the dehydration of hydrated salts is of relevance because it directly influences the thermal protection capacity of gypsum-based systems. During fire exposure, the release of chemically bound water acts as an effective heat sink and contributes to delaying temperature rise within the material. The kinetics of the dehydration reaction therefore determine both the rate of water release and the duration of the endothermic heat absorption process. Materials exhibiting well-defined dehydration steps with predictable kinetic behaviour may therefore provide more reliable thermal buffering effects in fire scenarios. Conversely, complex multi-step dehydration processes may lead to broader temperature ranges over which water release occurs, potentially influencing the thermal response of gypsum products during prolonged fire exposure.

The results support a fire engineering relevant classification of additive behaviour by temperature range. CAS and ESM act primarily in the lower temperature interval where dehydration and bound water release occur early during heating, while ATH and MDH provide endothermic buffering at higher temperatures. This staging is valuable for gypsum-based assemblies where gypsum dehydration dominates below about 250 °C and additives can extend heat absorption to higher temperatures or increase the magnitude of the heat sink at earlier stages.

The enthalpy ranking indicates that ATH, MDH, and ESM provide larger endothermic capacity per unit mass than CAS in the tested conditions. In a gypsum-based composite, this supports additive selection strategies that target either early-stage dehydration buffering (ESM, CAS) or high temperature buffering (ATH, MDH), subject to compatibility, durability, and mechanical constraints.

The kinetic triplets derived here are intended to be used as source terms in coupled heat transfer and dehydration models for gypsum-based assemblies. A proposed workflow to be followed in fire simulations of gypsum-based assemblies is the following:

1. Select the material layer model (1D wall model, finite element heat transfer model, or coupled CFD boundary material model).
2. Assign thermal properties and, where appropriate, their temperature dependence.
3. Implement dehydration steps using Table 3 kinetic triplets and Table 2 dehydration enthalpies. For CAS and ESM, implement the multi step structure with weights w_r.
4. Validate the implementation by reproducing non isothermal DSC conversion curves under the same heating rates, then run the intended fire exposure history (standard fire curve or parametric fire).
5. Perform sensitivity checks on step weighting and on the effective nature of the kinetics when transferring from DSC boundary conditions to porous assembly environments.

This workflow supports performance based assessment where dehydration heat sinks and staged water release influence predicted temperatures at interfaces and on protected structural members, consistent with established gypsum board modelling approaches [4–6,10].

6.3. Practical Limitations and Transferability

The findings of this study provide useful insights for the development of improved thermal decomposition models for gypsum-based materials and other mineral systems used in fire protection applications. Accurate kinetic parameters are essential for numerical simulations that aim to predict the thermal response of building materials under fire conditions. Incorporating experimentally derived kinetic parameters and appropriate reaction models can therefore contribute to more reliable fire performance predictions.

The kinetic parameters should be interpreted as effective values derived under restricted vapor exchange in pinhole crucibles. In real gypsum boards, local vapor pressure and transport pathways

 doi:10.20944/preprints202603.0582.v1

depend on pore structure, cracking, paper facings, and boundary conditions. Consequently, the parameters are best used within models that can accommodate effective kinetics and are validated at the assembly scale when possible. For ATH, the use of gypsum board containing 5 wt.% ATH implies that extracted kinetics represent the additive response within that matrix and may differ from intrinsic ATH kinetics measured as a pure powder.

Future studies could investigate the dehydration behaviour of these systems under conditions that more closely resemble realistic fire exposure and explore the integration of the derived kinetic parameters into coupled thermo-chemical fire models.

7. Conclusions

This study investigated the dehydration kinetics of selected non-organic salts—aluminium trihydrate (ATH), magnesium hydroxide (MDH), calcium aluminate sulphate (CAS), and magnesium sulphate heptahydrate (ESM)—under elevated temperature conditions using differential scanning calorimetry (DSC). Measurements were performed at different heating rates up to 600 °C using pinhole crucibles to simulate autogenous water vapor pressure.

The DSC results revealed that ATH, MDH, and CAS exhibit single-stage dehydration behavior, whereas ESM undergoes a complex, multi-step dehydration process involving the sequential release of water and the formation of intermediate meta-stable hydrates. Among the examined salts, ATH, MDH, and ESM demonstrated higher energy absorption per unit mass compared to CAS, suggesting their greater potential as flame-retardant additives.

To resolve overlapping thermal events and support kinetic interpretation, peak deconvolution techniques (e.g., Fraser–Suzuki function) were employed. Kinetic parameters were extracted using both model-free and model-fitting approaches. The activation energy profiles indicated that ATH and MDH follow single-step mechanisms, while CAS and ESM involve multiple steps—despite the initial impression from DSC alone suggesting otherwise for CAS.

All reactions—both single- and multi-step—were consistently modeled using the Avrami–Erofeev framework, which reflects nucleation and growth mechanisms. This is in agreement with the literature and supported by prior findings on hydrate decomposition pathways. The use of empirical models such as the Sesták–Berggren equation in future work may provide further flexibility in capturing overlapping reaction mechanisms.

Finally, model predictions for conversion fraction and reaction rates, based on the extracted kinetic parameters (Table 3), matched the experimental DSC data with high accuracy. These results support the reliability and applicability of the derived kinetic triplets for use in fire modeling and material performance assessments. The findings also align with earlier studies emphasizing the critical influence of water vapor pressure on phase stability and transformation rates.

Beyond advancing the characterization of hydrated salts, the present findings support the broader objectives of fire science by enabling more reliable modelling of gypsum-based systems exposed to realistic fire scenarios. The derived kinetic parameters and validated numerical predictions offer practical inputs for performance-based fire engineering, contributing to safer building design and improved assessment of material behaviour during fire events. By connecting experimental thermal analysis with predictive modelling approaches, the paper aligns with current efforts to understand how fire dynamics interact with construction materials, infrastructure resilience, and community safety within the built environment. Such predictive capabilities are critical for modern fire engineering approaches that rely on physics based assessment rather than prescriptive testing alone. By enabling more accurate evaluation of passive fire protection behaviour under realistic thermal loads, the present work contributes to safer building design and aligns with the multidisciplinary scope of fire science that integrates technology, engineering practice, and societal resilience

Author Contributions: Conceptualization, M.P., D.K. and M.F.; methodology, M.P.; validation, M.P. and D.K.; formal analysis, M.P.; investigation, M.P., D.D. and M.M.; data curation, M.P.; writing—original draft

 doi:10.20944/preprints202603.0582.v1

preparation, M.P.; writing—review and editing, M.P., D.K. and M.F.; visualization, M.P.; supervision, D.K. and M.F.; project administration, M.F. All authors have read and agreed to the published version of the manuscript.

Funding: This research received no external funding.

Institutional Review Board Statement: Not applicable.

Informed Consent Statement: Not applicable.

Data Availability Statement: The data presented in this study are available on request from the corresponding author.

Acknowledgments: The authors gratefully acknowledge Knauf Gips KG for providing the gypsum-based materials used in this study.

Conflicts of Interest: The authors declare no conflicts of interest.

Abbreviations

The following abbreviations are used in this manuscript:

ATH	Aluminium Trihydrate ($Al(OH)_3$)
ESM	Magnesium Sulphate Heptahydrate ($MgSO_4*7H2O$)
CAS	Calcium Aluminium Sulphate ($3CaO*Al_2O_3*3CaSO_4*32H_2O$)
MDH	Magnesium Hydroxide ($Mg(OH)_2$)
ICTAC	International Confederation for Thermal Analysis and Calorimetry
k	reaction rate constant
L_v	enthalpy of evaporation, 2260000
N_R	number of reactions
P	pressure
R_g	universal gas constant, 8.314
t	time
T	temperature
w	weight factor
Greek symbols	
α	conversion fraction
ΔH	enthalpy of reaction
Subscripts	
dh	dehydration
r	reaction index
Special Symbols	
d	total derivative

References

1. Ang, C.N.; Wang, Y.C. Effect of Moisture Transfer on Specific Heat of Gypsum Plasterboard at High Temperatures. *Construction and Building Materials* **2009**, *23*, 675–686, doi:https://doi.org/10.1016/j.conbuildmat.2008.02.016.
2. Belmiloudi, A.; Le Meur, G. Mathematical and Numerical Analysis of Dehydratation of Gypsum Plasterboards Exposed to Fire. *Applied Mathematics and Computation* **2005**, *163*, 1023–1041, doi:https://doi.org/10.1016/j.amc.2004.06.013.

 doi:10.20944/preprints202603.0582.v1

3. Manzello, S.L.; Gann, R.G.; Kukuck, S.R.; Lenhert, D.B. Influence of Gypsum Board Type (X or C) on Real Fire Performance of Partition Assemblies. *Fire and Materials* **2006**, *31*, 425–442, doi:https://doi.org/10.1002/fam.940.
4. Mehaffey, J.R.; Cuerrier, P.; Carisse, G. A Model for Predicting Heat Transfer through Gypsum-Board/Wood-Stud Walls Exposed to Fire. *Fire and Materials* **1994**, *18*, 297–305, doi:https://doi.org/10.1002/fam.810180505.
5. Ghazi Wakili, K.; Hugi, E.; Wullschleger, L.; Frank, T.H. Gypsum Board in Fire — Modeling and Experimental Validation. *Journal of Fire Sciences* **2007**, *25*, 267–282, doi:10.1177/0734904107072883.
6. Kontogeorgos, D.A.; Founti, M.A. Gypsum Board Reaction Kinetics at Elevated Temperatures. *Thermochimica Acta* **2012**, *529*, 6–13, doi:https://doi.org/10.1016/j.tca.2011.11.014.
7. Ghazi Wakili, K.; Hugi, E. Four Types of Gypsum Plaster Boards and Their Thermophysical Properties under Fire Condition. *Journal of Fire Sciences* **2009**, *27*, 27–43, doi:10.1177/0734904108094514.
8. Zehfuß, J.; Sander, L. Gypsum Plasterboards under Natural Fire—Experimental Investigations of Thermal Properties. *Civil Engineering Design* **2021**, *3*, 62–72, doi:https://doi.org/10.1002/cend.202100002.
9. Kontogeorgos, D.; Mandilaras, I.; Founti, M. Scrutinizing Gypsum Board Thermal Performance at Dehydration Temperatures. *Journal of Fire Sciences - J FIRE SCI* **2011**, *29*, 111–130, doi:10.1177/0734904110381731.
10. Sam, V.S.; Nammalvar, A.; Iswarary, A.; Andrushia, D.; Ananthi, G.B.G.; Roy, K. Effect of Protective Coatings on Post-Fire Performance and Behavior of Mild Steel-Based Cold-Formed Steel Back-to-Back Channel Columns with Bolted Connections. *Fire* **2025**, *8*, doi:10.3390/fire8030107.
11. Manzello, S.L.; Gann, R.G.; Kukuck, S.R.; Prasad, K.; Jones, W.W. Performance of a Non-Load-Bearing Steel Stud Gypsum Board Wall Assembly: Experiments and Modelling. *Fire and Materials* **2006**, *31*, 297–310, doi:https://doi.org/10.1002/fam.939.
12. Han, X.C.; Xu, H.J.; Hua, W.S. Decomposition Performance and Kinetics Analysis of Magnesium Hydroxide Regulated with C/N/Ti/Si Additives for Thermochemical Heat Storage. *Applied Energy* **2023**, *344*, 121322, doi:https://doi.org/10.1016/j.apenergy.2023.121322.
13. Chen, B.; Kuznik, F.; Horgnies, M.; Johannes, K.; Morin, V.; Gengembre, E. Physicochemical Properties of Ettringite/Meta-Ettringite for Thermal Energy Storage: Review. *Solar Energy Materials and Solar Cells* **2019**, *193*, 320–334, doi:https://doi.org/10.1016/j.solmat.2018.12.013.
14. Miller, N.; Coffey, P.; Badenhorst, H.; Martin, P. The Effect of the Salt Precursor on the Particle Morphology and Thermal Properties of Magnesium Hydroxide for Thermochemical Energy Storage. *Journal of Energy Storage* **2021**, *44*, 103335, doi:https://doi.org/10.1016/j.est.2021.103335.
15. Slimani, H.; Ait Ousaleh, H.; El Harrak, A.; Linder, M.; Faik, A. Doping Effects on Magnesium Hydroxide: Enhancing Dehydration and Hydration Performance for Thermochemical Energy Storage Applications. *Chemical Engineering Journal* **2024**, *488*, 151048, doi:https://doi.org/10.1016/j.cej.2024.151048.
16. Ings, J.B.; Brown, P.W. An Evaluation of Hydrated Calcium Aluminate Compounds as Energy Storage Media: 1982.
17. Struble, L.J.; Brown, P.W. *Evaluation of Ettringite and Related Compounds for Use in Solar Energy Storage. Progress Report*; National Engineering Lab. (NBS), Washington, DC (USA): United States, 1984;
18. Struble, L.J.; Brown, P.W. Heats of Dehydration and Specific Heats of Compounds Found in Concrete and Their Potential for Thermal Energy Storage. *Solar Energy Materials* **1986**, *14*, 1–12, doi:https://doi.org/10.1016/0165-1633(86)90008-0.
19. Vladimir, Š.; Vepřek, O. Thermal Decomposition of Ettringite under Hydrothermal Conditions. *Journal of the American Ceramic Society* **1975**, *58*, 357–359, doi:https://doi.org/10.1111/j.1151-2916.1975.tb11513.x.
20. Rubinaite, D.; Dambrauskas, T.; Baltakys, K.; Siauciunas, R. Influence of Water Vapour Pressure on the Carbonation Process of Calcium Monosulfoaluminate 12-Hydrate. *Journal of Thermal Analysis and Calorimetry* **2024**, *150*, doi:10.1007/s10973-024-13233-1.
21. Nazrun, T.; Hassan, M.K.; Hasnat, M.R.; Hossain, M.D.; Ahmed, B.; Saha, S. A Comprehensive Review on Intumescent Coatings: Formulation, Manufacturing Methods, Research Development, and Issues. *Fire* **2025**, *8*, doi:10.3390/fire8040155.

 doi:10.20944/preprints202603.0582.v1

22. Kontogeorgos, D.; Mandilaras, I.; Founti, M. Scrutinizing Gypsum Board Thermal Performance at Dehydration Temperatures. *Journal of Fire Sciences - J FIRE SCI* **2011**, *29*, 111–130, doi:10.1177/0734904110381731.
23. Elbasuney, S. Novel Multi-Component Flame Retardant System Based on Nanoscopic Aluminium-Trihydroxide (ATH). *Powder Technology* **2017**, *305*, 538–545, doi:https://doi.org/10.1016/j.powtec.2016.10.038.
24. Duquesne, S.; Fontaine, G.; Cérin-Delaval, O.; Gardelle, B.; Tricot, G.; Bourbigot, S. Study of the Thermal Degradation of an Aluminium Phosphinate–Aluminium Trihydrate Combination. *Thermochimica Acta* **2013**, *551*, 175–183, doi:https://doi.org/10.1016/j.tca.2012.10.025.
25. Rothon, R.N. Mineral Fillers in Thermoplastics: Filler Manufacture and Characterisation. In *Mineral fillers in thermoplastics I: Raw materials and processing*; Jancar, J., Fekete, E., Hornsby, P.R., Jancar, J., Pukánszky, B., Rothon, R.N., Eds.; Springer Berlin Heidelberg: Berlin, Heidelberg, 1999; pp. 67–107 ISBN 978-3-540-69220-1.
26. Sabet, M.; Hassan, A.; Wahit, M.U.; Ratnam, C.T. Thermal Characterization of Alumina Trihydrate (ATH) and Flammability Studies of ATH Filled Low Density Polyethylene. *Journal of Information Technology & Multimedia* **2009**, *18*, 41–50.
27. Perković, N.; Rajčić, V.; Barbalić, J. Fire Resilience of Load-Bearing Wall Made of Hollow Timber Elements. *Fire* **2024**, *7*, doi:10.3390/fire7120433.
28. Hull, T.R.; Witkowski, A.; Hollingbery, L. Fire Retardant Action of Mineral Fillers. *Polymer Degradation and Stability* **2011**, *96*, 1462–1469, doi:https://doi.org/10.1016/j.polymdegradstab.2011.05.006.
29. Girardin, B.; Fontaine, G.; Duquesne, S.; Försth, M.; Bourbigot, S. Measurement of Kinetics and Thermodynamics of the Thermal Degradation for Flame Retarded Materials: Application to EVA/ATH/NC. *Journal of Analytical and Applied Pyrolysis* **2017**, *124*, 130–148, doi:https://doi.org/10.1016/j.jaap.2016.12.034.
30. Camino, G.; Maffezzoli, A.; Braglia, M.; De Lazzaro, M.; Zammarano, M. Effect of Hydroxides and Hydroxycarbonate Structure on Fire Retardant Effectiveness and Mechanical Properties in Ethylene-Vinyl Acetate Copolymer. *Polymer Degradation and Stability* **2001**, *74*, 457–464, doi:https://doi.org/10.1016/S0141-3910(01)00167-7.
31. Dzidziguri, E.; Vasilev, A.; Ozherelkov, D.; Pelevin, I.; Zotov, B.; Федоренко, Л.; Gromov, A. Thermal Decomposition of Chemically Precipitated Nanopowder of Aluminum Hydroxide. *Physics and Chemistry of Materials Treatment* **2022**, *5*, 39–46, doi:10.30791/0015-3214-2022-5-39-46.
32. Sain, M.; Park, S.H.; Suhara, F.; Law, S. Flame Retardant and Mechanical Properties of Natural Fibre–PP Composites Containing Magnesium Hydroxide. *Polymer Degradation and Stability* **2004**, *83*, 363–367, doi:https://doi.org/10.1016/S0141-3910(03)00280-5.
33. N'Tsoukpoe, K.E.; Schmidt, T.; Rammelberg, H.U.; Watts, B.A.; Ruck, W.K.L. A Systematic Multi-Step Screening of Numerous Salt Hydrates for Low Temperature Thermochemical Energy Storage. *Applied Energy* **2014**, *124*, 1–16, doi:https://doi.org/10.1016/j.apenergy.2014.02.053.
34. Paulik, J.; Paulik, F.; Arnold, M. Dehydration of Magnesium Sulphate Heptahydrate Investigated by Quasi Isothermal—Quasi Isobaric TG. *Thermochimica Acta* **1981**, *50*, 105–110, doi:https://doi.org/10.1016/0040-6031(81)85048-4.
35. Van essen, M.; Zondag, H.A.; Schuitema, R.; Helden, W.; Rindt, C. Materials for Thermochemical Storage: Characterization of Magnesium Sulfate. *Proc Eurosun* **2008**.
36. Emons, H.H.; Ziegenbalg, G.; Naumann, R.; Paulik, F. Thermal Decomposition of the Magnesium Sulphate Hydrates under Quasi-Isothermal and Quasi-Isobaric Conditions. *Journal of Thermal Analysis and Calorimetry* **1990**, *36*, 1265–1279, doi:10.1007/bf01914050.
37. Wagman, D.D.; Evans, W.H.; Parker, V.B.; Schumm, R.H.; Halow, I.; Bailey, S.M.; Churney, K.L.; Nuttall, R.L. The NBS Tables of Chemical Thermodynamic Properties: Selected Values for Inorganic and C1 and C2 Organic Substances in SI Units. *Journal of Physical and Chemical Reference Data* **1982**, *11*.
38. Phadnis, A.B.; Deshpande, V.V. On the Dehydration of MgSO4 · 7 H2O. *Thermochimica Acta* **1981**, doi:10.1016/0040-6031(81)80016-0.
39. Shahzad, M.; Sultan, F. Complex Reactions and Dynamics. In *Advanced chemical kinetics*; Farrukh, M.A., Ed.; IntechOpen: Rijeka, 2017.

 doi:10.20944/preprints202603.0582.v1

40. Vyazovkin, S.; Burnham, A.K.; Criado, J.M.; Pérez-Maqueda, L.A.; Popescu, C.; Sbirrazzuoli, N. ICTAC Kinetics Committee Recommendations for Performing Kinetic Computations on Thermal Analysis Data. *Thermochimica Acta* **2011**, *520*, 1–19, doi:https://doi.org/10.1016/j.tca.2011.03.034.
41. Vyazovkin, S.; Dollimore, D. Linear and Nonlinear Procedures in Isoconversional Computations of the Activation Energy of Nonisothermal Reactions in Solids. *Journal of Chemical Information and Computer Sciences* **1996**, *36*, 42–45, doi:10.1021/ci950062m.
42. Vyazovkin, S.; Wight, C.A. Model-Free and Model-Fitting Approaches to Kinetic Analysis of Isothermal and Nonisothermal Data. *Thermochimica Acta* **1999**, *340–341*, 53–68, doi:https://doi.org/10.1016/S0040-6031(99)00253-1.
43. Brown, M.E.; Maciejewski, M.; Vyazovkin, S.; Nomen, R.; Sempere, J.; Burnham, A.; Opfermann, J.; Strey, R.; Anderson, H.L.; Kemmler, A.; et al. Computational Aspects of Kinetic Analysis: Part A: The ICTAC Kinetics Project-Data, Methods and Results. *Thermochimica Acta* **2000**, *355*, 125–143, doi:https://doi.org/10.1016/S0040-6031(00)00443-3.
44. Kontogeorgos, D.A.; Founti, M.A. Gypsum Board Reaction Kinetics at Elevated Temperatures. *Thermochimica Acta* **2012**, *529*, 6–13, doi:https://doi.org/10.1016/j.tca.2011.11.014.
45. Braga, R.; Melo, D.; Aquino, F.; Freitas, J.; Melo, M.; Barros, J.; Fontes, M. Characterization and Comparative Study of Pyrolysis Kinetics of the Rice Husk and the Elephant Grass. *Journal of Thermal Analysis and Calorimetry* **2014**, *115*, doi:10.1007/s10973-013-3503-7.
46. Dubey, G.; Vairakannu, P.; Tiwari, P. TGA-Based Kinetic Parameters and Laboratory-Scale Pyrolysis of Northeastern Indian Coals. *Journal of Thermal Analysis and Calorimetry* **2025**, *150*, doi:10.1007/s10973-025-14203-x.
47. N.V., S.; Muraleedharan, K. Kinetic Study of the Multistep Thermal Behaviour of Barium Titanyl Oxalate Prepared via Chemical Precipitation Method. *Journal of Thermal Analysis and Calorimetry* **2018**, *136*, doi:10.1007/s10973-018-7777-7.
48. Koga, N.; Šesták, J.; Šimon, P. Some Fundamental and Historical Aspects of Phenomenological Kinetics in the Solid State Studied by Thermal Analysis. In *Thermal analysis of micro, nano- and non-crystalline materials: Transformation, crystallization, kinetics and thermodynamics*; Šesták, J., Šimon, P., Eds.; Springer Netherlands: Dordrecht, 2013; pp. 1–28 ISBN 978-90-481-3150-1.